

Geophysical Research Letters[®]



RESEARCH LETTER

10.1029/2022GL102678

Key Points:

- We first observed shallow tremors by distributed acoustic sensing (DAS) using offshore fiber-optic cable in the Nankai Trough
- Tremor signals of DAS are composed of several phases of variable apparent velocities that are coherent only in tens of meters
- Spatial relationship between shallow tremors and subducted seamount is suggested along the dip direction

Supporting Information:

Supporting Information may be found in the online version of this article.

Correspondence to:








S. Baba,
babasatoru@jamstec.go.jp

Citation:

Baba, S., Araki, E., Yamamoto, Y., Hori, T., Fujie, G., Nakamura, Y., et al. (2023). Observation of shallow slow earthquakes by distributed acoustic sensing using offshore fiber-optic cable in the Nankai Trough, southwest Japan. *Geophysical Research Letters*, 50, e2022GL102678. <https://doi.org/10.1029/2022GL102678>

Received 4 JAN 2023
Accepted 21 MAY 2023

Observation of Shallow Slow Earthquakes by Distributed Acoustic Sensing Using Offshore Fiber-Optic Cable in the Nankai Trough, Southwest Japan

Satoru Baba¹ , Eiichiro Araki¹ , Yojiro Yamamoto¹ , Takane Hori¹ , Gou Fujie¹ , Yasuyuki Nakamura¹ , Takashi Yokobiki¹, and Hiroyuki Matsumoto¹ 

¹Japan Agency for Marine-Earth Science and Technology, Yokosuka, Japan

Abstract Off Cape Muroto area, along the Nankai Trough in southwest Japan, is a typical area with adjacent occurrences of slow and megathrust earthquakes. High-resolution monitoring of slow earthquakes is necessary to understand tectonic conditions. In the off Muroto area, distributed acoustic sensing (DAS) measurement, which provides high-density strain data, has been conducted using offshore fiber-optic cable. We observed shallow tremors, a type of slow earthquakes, using DAS measurement for the first time. The characteristics of the tremor signals recorded by DAS were longer durations than those recorded in seismographs and composed of several phases with apparent velocities of several hundreds of m/s to several km/s that are coherent only in tens of meters. By combining DAS and seismograph data, we located these tremors around a subducted seamount peak. Therefore, spatial relationship between slow earthquakes and structural characteristics is suggested. This is a pioneering study of slow earthquake observation using DAS.

Plain Language Summary Distributed acoustic sensing (DAS) measurement is a recent technology that uses a fiber-optic cable as a strain sensor array. As DAS provides high-density observation data, it has often been used for the observation of regular earthquakes in recent years. However, few studies have used DAS measurement to observe slow earthquakes, which have longer characteristic durations compared to regular earthquakes. We observed shallow tremors, a type of slow earthquake, using DAS for the first time off Cape Muroto, where slow and huge regular earthquakes occur in the neighboring areas. The characteristics of tremor signals in DAS data are long durations and composition of several phases with variable apparent velocities that are coherent only in tens of meters. We located tremors by picking the arrival of signals by visually checking the waveforms of DAS and an offshore seismograph network and locating them at the point where the difference between synthetic and observed arrival times was the smallest. Most tremors occurred around 134.7°E, 32.8°N, which corresponds to a subducted seamount peak; therefore, a spatial relationship between slow earthquakes and a subducted seamount is suggested in this region.

1. Introduction

Recently, slow earthquakes, which have longer characteristic durations than regular earthquakes of the same seismic moment (Ide et al., 2007), have been observed around the rupture zones of megathrust earthquakes on the plate boundary mainly in subduction zones. Slow earthquakes are classified as tremors (observed in a frequency range of 2–8 Hz; e.g., Obara, 2002), very low frequency earthquakes (VLFs; observed in a frequency range of 0.02–0.05 Hz; e.g., Obara & Ito, 2005), and slow slip events with durations of several days to years (e.g., Dragert et al., 2001; Hirose et al., 1999). Tremors and VLFs are often correlated spatiotemporally (e.g., Ito et al., 2007). In addition, slow earthquake signals were found in the frequency band between tremors and VLFs (Kaneko et al., 2018; Masuda et al., 2020; Yamashita et al., 2021). Therefore, slow earthquakes are considered broadband phenomena. Slow earthquakes can be a stress meter on the plate boundary (Obara & Kato, 2016) and have the potential to trigger megathrust earthquakes (e.g., Kato et al., 2012; Vaca et al., 2018). Therefore, investigation of the spatial variation in slow earthquake activity is important for understanding tectonic conditions on the plate boundary.

Along the Nankai Trough, where the Philippine Sea plate subducts, megathrust earthquakes with Mw of ~8 have occurred repeatedly with a recurrence interval of 100–200 years (Ando, 1975). Around the coseismic slip areas of these megathrust earthquakes, slow earthquakes have also been observed. The off Cape Muroto area is a part of the coseismic slip area of these megathrust earthquakes (Figure 1). In this area, shallow slow earthquakes

© 2023. The Authors.

This is an open access article under the terms of the [Creative Commons Attribution License](https://creativecommons.org/licenses/by/4.0/), which permits use, distribution and reproduction in any medium, provided the original work is properly cited.

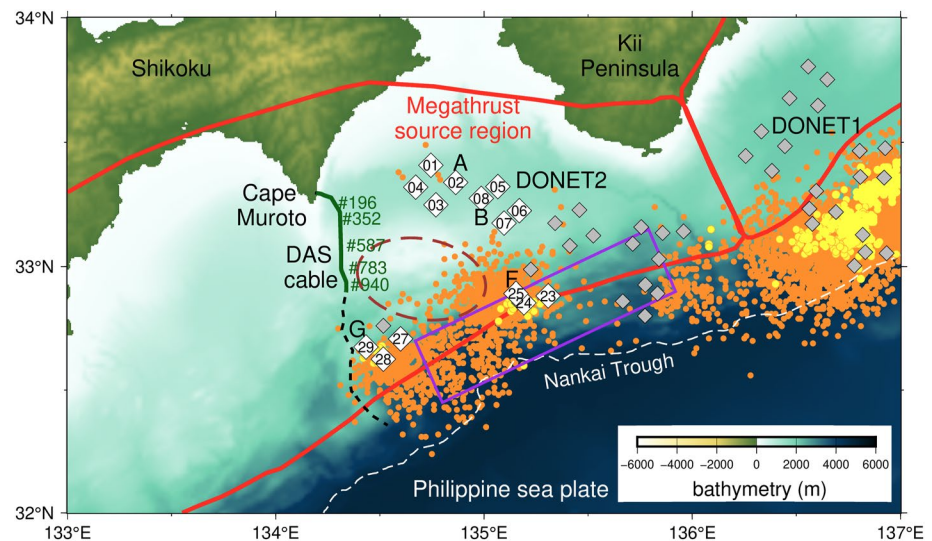


Figure 1. Tectonics along the Nankai Trough. Orange dots are epicenters of tremors detected by Tamaribuchi et al. (2022). Yellow dots are epicenters of shallow very low frequency earthquakes detected by Nakano et al. (2018) and Yamamoto et al. (2022). The purple rectangle represents an estimated slow slip event fault plane in 2017–2018 (Yokota & Ishikawa, 2020). Dashed black lines and solid green lines represent the sections of the Muroto cable that are not used and used for the distributed acoustic sensing measurements in this study, respectively. White and gray diamonds show the locations of DONET2 stations used and not used for this study, respectively. Letters A, B, F, and G represent the node names of DONET2. The brown ellipse shows the location of a subducted seamount (Kodaira et al., 2000). Red polygons indicate the anticipated megathrust source regions (Earthquake Research Committee, 2001). The white dashed line indicates the Nankai Trough. Background color scale denotes the bathymetry (ETOPO1; Amante & Eakins, 2009).

have been detected in the updip of the coseismic slip area (e.g., Nakano et al., 2018; Takemura et al., 2019; Tamaribuchi et al., 2022; Yokota & Ishikawa, 2020) by both onshore and offshore data (e.g., Dense Ocean floor Network system for Earthquakes and Tsunamis 2 (DONET2); Aoi et al., 2020; Kaneda et al., 2015; National Research Institute for Earth Science and Disaster Resilience, 2019). Thus, this area is a typical example of adjacent occurrences of slow and megathrust earthquakes. In addition, a seamount is subducted in this area (e.g., Kodaira et al., 2000); therefore, the geometry of the plate boundary is characteristic. However, the detection and locations of shallow slow earthquakes by previous studies in this area are limited and scattered (Figure 1) because of the difficulty of offshore observation due to the long distances from the onshore network, noisy offshore data, and the limited spatial distributions of the offshore data. Therefore, shallow slow earthquake activity has not been understood with a high resolution compared to deep slow earthquake activity, which occurs in the downdip area. In addition, characteristics of tremor signals have not been discussed well by the dense observation. To investigate the distribution of shallow slow earthquake activity and detailed characteristics of their waveforms, observations with offshore data are required.

Recently, distributed acoustic sensing (DAS) measurement has been widely used for the observations of regular earthquakes (e.g., Lindsey et al., 2017; Shinohara et al., 2022; Zhan, 2019), infragravity waves (Williams et al., 2019), hydroacoustic signals (Matsumoto et al., 2021), and the extraction of *P*-waves from ambient noise (Tonegawa et al., 2022). DAS measurements use an optic fiber cable as a strain or strain rate sensor array. The strain or strain rate data can be obtained at many locations along the fiber-optic cable with intervals of meter scale and at a high sampling rate (500–1,000 samples per second). Therefore, DAS measurements enable high-density spatiotemporal observations. Although DAS measurement is commonly used to observe regular earthquakes, there are few studies of slow earthquake observations with the DAS measurement. Currently, the Japan Agency for Marine-Earth Science and Technology conducts real-time DAS observations off Cape Muroto, using an offshore fiber-optic cable along the dip direction. As the fiber-optic cable exists near the shallow slow earthquake area, the spatial distribution of slow earthquake activity can be investigated with high-density DAS data.

To clarify detailed characteristics of waveforms and the distribution of shallow slow earthquakes off Cape Muroto, we used DAS measurement to observe shallow tremors. As this is the first study of tremor observation using DAS, we have discussed the characteristics of strain waveforms recorded by DAS and compared the

waveforms of DAS and seismometers. We then investigated the hypocenters of shallow tremors by using the data from the DAS and DONET2 broadband seismometers. Finally, we have presented the advantages, challenges, and prospects of slow earthquake observations using DAS measurement. This study can be a pioneering study of slow earthquake observations using DAS.

2. Observation of Tremor Signals by DAS Measurement

2.1. Data

For the DAS observation, we used the Muroto cable with a total length of 128 km. Details of the Muroto cable are described in Ide et al. (2021) and Matsumoto et al. (2021). The DAS measurement is conducted by AP Sensing with a sensing length of 55 km along the cable from the coast. The gauge length, the sensor spacing, and the sampling rate of the original data are 40.8 m, 5.1 m, and 500 Hz, respectively. In the DAS measurement, the temporal change in strain rate converted from the differential phase at each channel is recorded. We prepared decimated data by stacking and averaging the waveforms of successive 10 channels to downsample to 51-m channel spacing and decimating to 100 Hz sampling. The temporal change in strain rate has been continuously recorded by the DAS measurement since 29 January 2022.

2.2. Characteristics of Tremor Signals Measured Using DAS

The plots of the DAS strain rate records at all channels of the decimated data in a frequency range of 2–10 Hz demonstrate a signal propagating from south to north during the period from January 30 to 8 February 2022 (Figure 2a). During this time window, tremor signals were shown to simultaneously occur in the broadband seismograms of DONET2 in the same frequency range (Figures S1a–S1c in Supporting Information S1). Therefore, the signal in the DAS records shown in Figure 2a is considered a tremor signal. We found 29 tremor signals during the period by visually checking the plots of DAS records from January to March 2022 (Data Set S1).

We investigated the detailed characteristics of the tremor signals by plotting the temporal strain change, which was obtained by integrating the raw strain rate data (Figure 2b). A tremor signal is composed of several phases with variable apparent velocities, each with a duration of several seconds. These phases were coherent within only tens of meters (Figure S2 in Supporting Information S1). This characteristic may be caused by structural heterogeneity in the sediment with a scale of ~10 m. The apparent phase velocity of these phases is evaluated to be the range between several hundreds of m/s and several km/s (Text S1 and Figure S3 in Supporting Information S1). The minimum value of the apparent phase velocity is 0.3 km/s.

The amplitudes of tremor signals in the frequency range of 2–10 Hz observed in the original channels were ~1 nstrain (Figure 2b and Figure S1b in Supporting Information S1). Assuming a plane wave, the velocity waveforms can be calculated by multiplying the apparent phase velocity by the strain waveform (e.g., Daley et al., 2016; Shinohara et al., 2022; Wang et al., 2018). The apparent phase velocity is evaluated to be the range between several hundreds of m/s and several km/s; therefore, the velocity amplitude is estimated to be several hundreds to thousands m/s. The amplitudes of the broadband seismograms at the A-node and G-node stations of DONET2, which are the nearest stations to the DAS cable, are 500 and 4,000 nm/s, respectively (Figure S1c in Supporting Information S1). If the tremor shown in Figure 2 occurs in the area where shallow tremors and VLFs were located in previous studies, the hypocentral distance of DAS cable is closer to A-node stations than G-node stations. The converted DAS amplitude of tremor signals with the phase velocity of hundreds of m/s is closer to velocity amplitudes in A-node stations than those with the phase velocity of several km/s. It suggests that tremor signals are dominantly composed of phases with velocity of hundreds of m/s.

As the tremor signals of DAS records are not coherent, we calculated the envelopes of strain waveforms from DAS records and velocity waveforms of broadband seismograms from DONET2 data to investigate the outline of tremor signals. After applying band-pass filtering with a frequency range of 2–8 Hz, we obtained envelope waveforms by squaring, low-pass filtering below 0.2 Hz, and resampling at one sample per second in a method similar to that of Ide (2010).

Generally, the duration of a tremor signal in DAS channels (40–60 s) is longer than that in horizontal components of DONET2 broadband seismometers with the similar hypocentral distances (30–50 s) (Figure 2c and Figure S4 in Supporting Information S1). The reason for long duration of tremor signals in DAS channels can be caused by

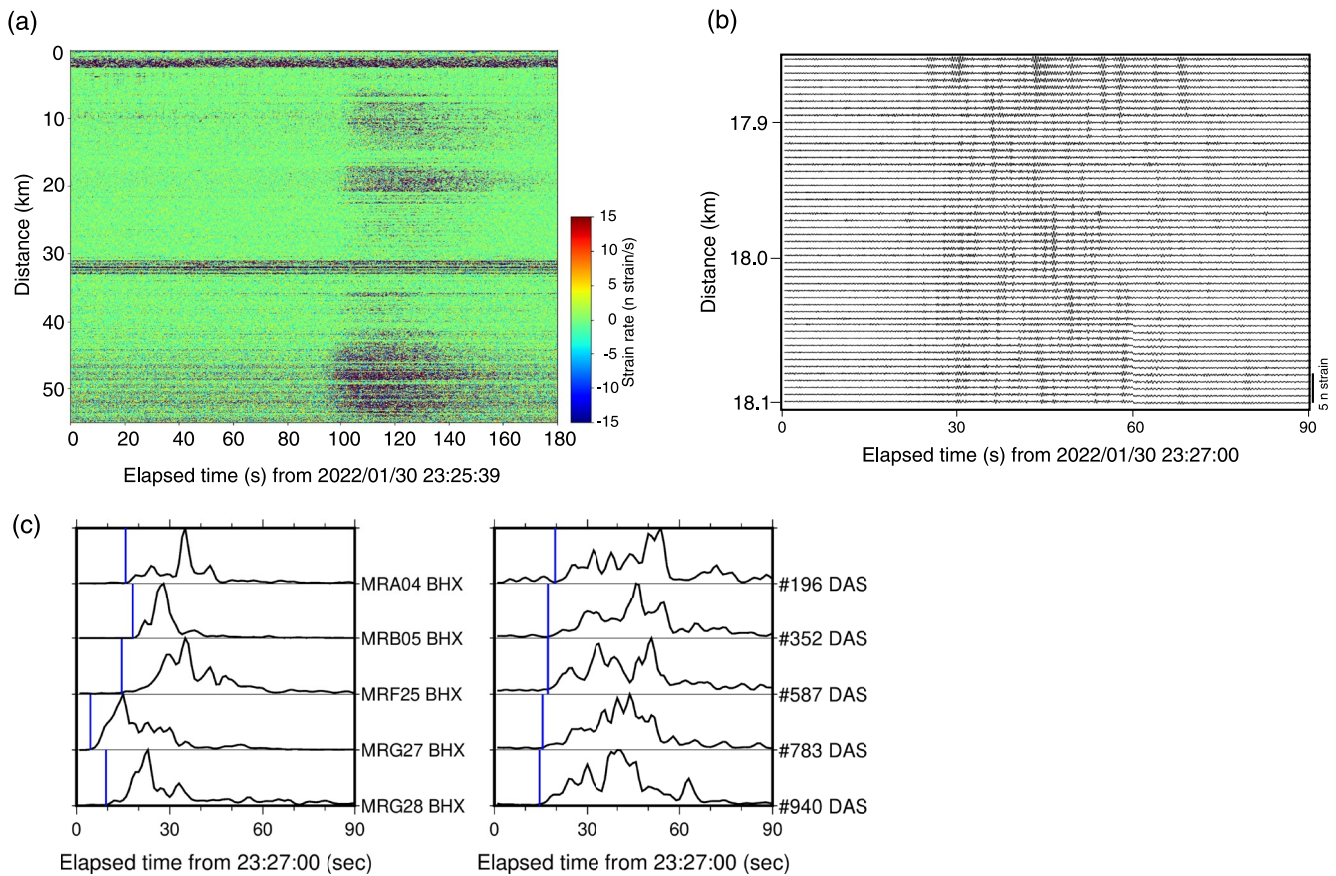


Figure 2. (a) Time-distance plot of decimated strain rate data from distributed acoustic sensing (DAS) measurement in a frequency range of 2–10 Hz when a tremor occurred. (b) Enlarged section of a time-distance plot of raw strain data in a frequency range of 2–10 Hz. (c) Example of envelope waveforms of a tremor normalized by the maximum amplitudes at DONET2 stations (left) and DAS channels (right). Blue lines show the picked arrival time of the tremor signal. Location of DAS channels are shown in Figure 1.

large amplitudes of *S*-coda waves. A possible reason is the difference in angle sensitivities between the DAS and horizontal components of seismometers. If we consider an *S*-wave with an incident angle of θ along a cable on the *x*-axis, the displacement in the *x*-direction is $\sin\theta$ times. Accordingly, the maximum amplitude occurs when the incident angle of an *S*-wave is 90° . On the other hand, the apparent velocity of this cable is $1/\cos\theta$ of the actual velocity; therefore, the weight of the strain of the *S*-wave is $\sin\theta \cos\theta$ ($=\sin 2\theta$). Accordingly, the maximum amplitude of the strain occurs when the incident angle is 45° . Therefore, DAS may measure scattered coda waves that are incident obliquely to the cable as large amplitudes. Another possible reason is the low phase velocity in the *S*-coda waves. If phase velocities of later *S*-coda waves of tremors are low, the velocity amplitudes of these phases in DONET are measured small. However, it cannot be denied that small-scale structural heterogeneities in the sediment affect the duration and shape of tremor signals in the envelopes of DAS channels apart from the nature of DAS measurement. To investigate the cause of differences in tremor signals between the DONET2 and DAS channels, observation of tremors in DAS and seismometers at the same position, simulation of strains in DAS channels, or detail investigation of phase velocity of tremor signals are required in the future works.

3. Distribution of Tremors Observed by the DAS Measurement

3.1. Method of Locating Tremors

We located 29 tremors observed by DAS measurement using DAS strain data and horizontal velocity waveforms of DONET2 broadband seismometers. As shown in Figure 2b, the tremor signals were not coherent; therefore, we used the envelopes obtained by the procedure described in Section 2.2 for the tremor location. We used the strain data of 55 DAS channels with intervals of 1 km and two horizontal components of broadband seismograph data of stations in the DONET2 A, B, F, and G nodes (Figure 1).

First, we manually picked the rising of envelopes of tremor signals in the DAS channels and horizontal channels of the DONET2 stations (Figure 2c and Figure S4 in Supporting Information S1), considering that the rising of the envelope corresponds to the arrival of *S*-wave. In some channels, the arrival of the tremor signals in the envelopes is unclear. In such a case, we did not pick the arrival. We set grids with 0.01° intervals on the top of the Philippine Sea plate (Nakanishi et al., 2018) and located tremor events at grid points where the residual between the observed and synthetic travel times was the smallest by the grid search. The residual is calculated using the following equation:

$$\text{Residual} = \sqrt{\frac{\sum_{i=1}^{N_{\text{DAS}}+N_{\text{DONET}}} w_i (t_i^{\text{obs}} - t_i^{\text{syn}})^2}{\sum_{i=1}^{N_{\text{DAS}}+N_{\text{DONET}}} w_i}}, \quad (1)$$

where t_i^{obs} and t_i^{syn} are the observed and synthetic travel times at i th channel, respectively, and N_{DAS} and N_{DONET} are the number of DAS and DONET2 channels where the arrival of the tremor signals can be picked, respectively. As the number of DAS channels is larger than that of the DONET2 channels, we introduced weight factor w_i to the weight of the DAS and DONET2 channels to 1:1 in Equation 1. The weight factor w_i is defined as $w_i = \frac{N_{\text{DONET}}}{N_{\text{DAS}} + N_{\text{DONET}}}$ for DAS channels and $w_i = \frac{N_{\text{DAS}}}{N_{\text{DAS}} + N_{\text{DONET}}}$ for DONET2 channels. The origin time was searched in the range from 30 s before to 5 s after the arrival times of the channels where the picked arrival time was first. Synthetic travel times were calculated based on a one-dimensional *S*-wave velocity structure model representing the area near the Nankai Trough (Nakano et al., 2013). To verify the effect of DAS data, we located the same tremor event using the same method with only DONET2 data (Data Set S2). In this case, the weight factor w_i is 1 for all channels.

In this study, we did not use the envelope correlation method, which is frequently used for tremor locations. Due to the variation in tremor signal duration and shape, the correlation coefficients between channel pairs are generally small; therefore, the travel time differences obtained by envelope correlation are not often consistent with those obtained by arrival times.

3.2. Method of Locating VLFs Correlated With Tremors

In the broadband seismometer data from G-node stations, VLF signals were also found in a frequency range of 0.02–0.05 Hz at the same time as tremor signals observed by DAS (Figure S1d in Supporting Information S1), although VLF signals were not found in data from the A-node stations. For 25 of the 29 tremors observed by DAS, the VLF signals were temporally correlated. We located these VLFs and determined their centroid moment tensor (CMT) solutions using the DONET2 data and the same method of Yamamoto et al. (2022) (the SWIFT system; Nakano et al., 2018). The parameter setting, calculation of synthetic waveforms, and used one-dimensional velocity structure (Nakano et al., 2013) are the same as Yamamoto et al. (2022). The location and CMT solutions of these VLFs are shown in Data Set S3.

3.3. Results

Most of the tremors were located northeast of the G-node of DONET2 around 134.7°E and 32.8°N (Figure 3a and Figure S5 in Supporting Information S1). Generally, the residual of tremor location is 2–3 s. According to the residual distribution (Figure S6 in Supporting Information S1), the resolution of the epicenters was considered to be 0.1–0.2°. Based on the residual distribution of the analysis with only DONET2 data, the location has a large uncertainty in the east-west direction north of the G-node (Figure S6b in Supporting Information S1). This uncertainty can be reduced by combining DAS and DONET2 data, because the DAS cable extends north of the G-node. The location estimated from DONET2 and DAS data tends to be slightly (~0.05°) more distant from the G-node than the location estimated from only DONET2 data. It is possible that the seismic wave velocity may be slower at the DAS channels; therefore, the arrival of the tremor signals may be delayed. Although there are tremors which were located outside the Nankai Trough, the residual of these tremors is large (>5 s); therefore, the uncertainty of locations of these tremors can be large.

Many VLFs which temporally correlated with tremors observed by DAS were also located northeast of the G-node (Figure 3a). Although the spatial distribution of tremors and VLFs partly overlapped, some of the VLFs that temporally correlated with tremors were located 0.1–0.2° closer to the G-node than tremors.

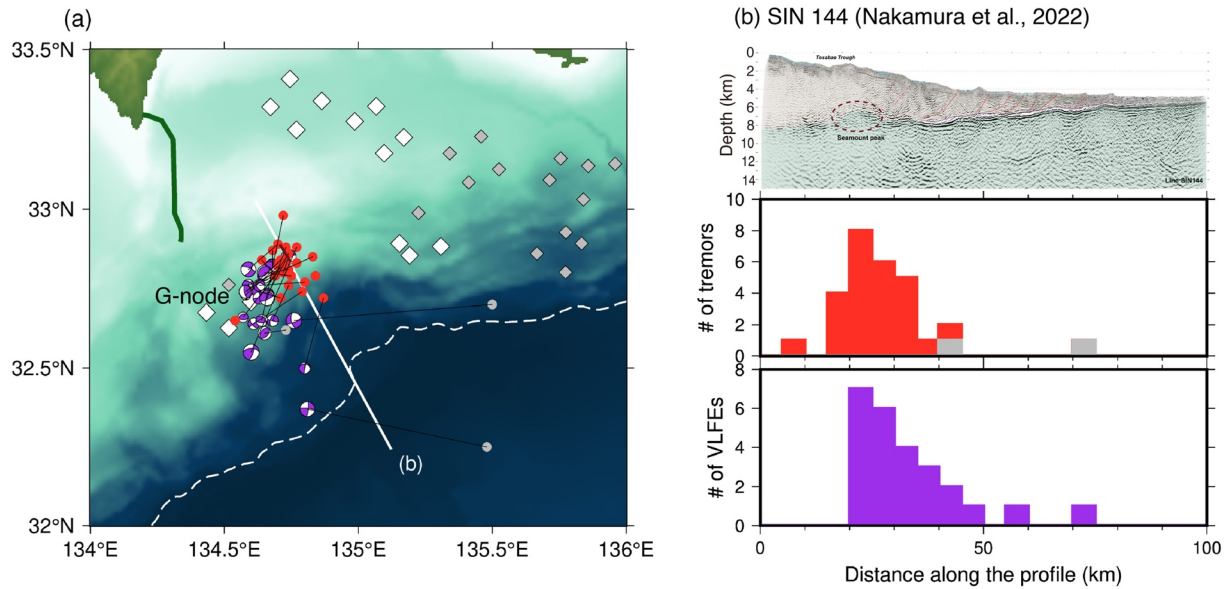


Figure 3. (a) Distribution of tremors located using both distributed acoustic sensing (DAS) and DONET2 data. Red and gray dots show the location of tremors with residual <5 s and >5 s. Purple beachballs represent very low frequency earthquakes (VLFs) which correspond to tremors observed by DAS. The corresponding tremor and VLF are connected by black lines. White line represents the profiles of SIN 144 in Nakamura et al. (2022). The brown area along the profile is the range of seamount (shown in panel (b)). Green line, white and gray diamonds, white dashed line and background color scaling are the same as displayed in Figure 1. (b) Profile of SIN 144 (referred from Nakamura et al., 2022) and cumulative numbers of tremors observed by DAS and VLFs which correspond to tremors along the profiles in the interval of 5 km. Numbers of tremors with residual <5 s and >5 s are shown as red and gray histograms, respectively. Number of VLFs is shown as purple histogram. The brown ellipse in panel (b) represents the seamount.

Although it is not clear whether VLFs and tremors occur at the same hypocenter, tremors and VLFs spatiotemporally correlated at a resolution of $0.1\text{--}0.2^\circ$. Most of VLFs were located only by G-node stations; therefore, the distance between the epicenters of the VLFs and the G-node may have a large uncertainty. Regarding the tremor locations, although there is an uncertainty of 2–5 s when manually picking, the difference between calculated and picked arrival time is generally smaller than 3 s (Figure S4 in Supporting Information S1). Considering the S-wave velocity (~ 3 km/s), this uncertainty corresponds to ~ 10 km ($\sim 0.1^\circ$). The discrepancy between tremor and VLF locations may be due to this uncertainty. Given the uncertainty of the tremor locations, it can be certain that most of tremors occur in the northeast of the G-node.

3.4. Correlation Between Tremor Distribution and Structures

To discuss the tectonic environment of slow earthquake activity, we compared the cumulative number of tremors and VLFs with the seismic reflection survey data of Line SIN144 (Nakamura et al., 2022; Figure 3). The number of tremors changes abruptly at 15 km along the profile SIN144. This profile is along the dip direction (Figure 3a); therefore, the downdip limit of tremor activity can be identified. The range of large numbers of tremors and VLFs were similar along the profile at a resolution of 5 km (Figure 3b).

Most of tremors occur near the peak of a seamount, and few tremors and VLFs occur in the downdip of the peak (Figure 3b). The relationship between shallow slow earthquake activity and subducted seamounts or ridges has been discussed in previous studies (e.g., Takemura et al., 2022; Toh et al., 2020). Sun et al. (2020) suggested that the updip of the seamount peak is a stress shadow with low effective normal stress, whereas the downdip is a high effective normal stress area. In the off Cape Muroto area, tremors and VLFs possibly occur in the stress shadow area of the updip area. On the other hand, accumulated stress can be released by high-speed ruptures of megathrust earthquakes in the downdip of the seamount peak. The spatial relationship between slow earthquakes and the seamount peak off Cape Muroto is consistent with Sun et al. (2020).

4. Advantages, Challenges, and Prospects of Slow Earthquake Observation by DAS

Seismic observation using DAS measurement is a recent technology. This is the first study to observe tremor signals using the DAS measurement; therefore, the advantages and disadvantages have not previously been

discussed extensively. In this section, we discuss the advantages, challenges, and prospects of slow earthquake observations using DAS measurement.

A major advantage of DAS measurement is its spatially dense observation. In this study, the characteristics of tremor signals that consist of several phases with velocity in the orders of several hundreds of m/s to several km/s and are coherent only in tens of meters are first clarified by DAS observation. The observation of tremors by DAS may reveal the detailed propagation characteristics of tremor signals.

However, it is difficult to locate events using DAS measurement with one linear cable. Like this study, a combination of DAS and other seismic network data is required. This disadvantage can be mitigated when the cable shape has a bending point. DAS array analysis using multiple cables in various directions can also be effective.

By comparing the DAS and DONET2 data, we found that the signal-to-noise ratio of DAS data was not higher than that of DONET2 data; therefore, detection ability cannot be improved by using DAS data. Thus, there are no events that are observed only in DAS data. In this observation, the sensing length of the DAS measurement did not reach the slow earthquake area. In addition, we could not find VLFE signals in the frequency range of 0.01–0.1 Hz in the DAS data for the observation period. In future works, conducting DAS measurement just above the slow earthquake area with an improved noise level in the lower frequency band by a more stable laser could enable the detection of more tremors and VLFs. This could further enhance the spatial resolution of slow earthquakes including their depths. By clarifying the tectonic environment and broadband characteristics of slow earthquakes in more detail using DAS observation, it is possible to approach the mechanisms of the occurrence of slow earthquakes.

As described in Section 2.2, the duration of tremor signals in DAS channels tended to be longer than those in the DONET2 data. In addition, the amplitude of the *P*-wave of regular earthquakes measured by DAS is relatively small owing to the high apparent velocity and near-vertical incident angle (Lior et al., 2021). Thus, the sensitivity of incident angles and high-amplitude phases can differ between DAS and seismometers. To apply the methods that have been used in seismology to the DAS data, it may be necessary to improve the methods that consider the properties of DAS measurement. The characteristics of DAS measurement should be investigated in future studies.

5. Conclusions

We observed shallow tremors by DAS measurement off Cape Muroto, southwest Japan, from January 30 to 8 February 2022. Although DAS measurement has recently been used for seismic observation, slow earthquake observations using DAS have been rare. The durations of tremors observed in the DAS channels were generally longer than those observed in DONET2 stations. In detail, tremor signals are composed of several phases with apparent velocities in the range of several hundred of m/s to several km/s, and these phases are coherent within only in tens of meters. We located these tremors by manually picking the rising of the envelopes of tremor signals at 2–8 Hz and searching for the point with the residual between synthetic and observed arrival times was the smallest. These tremors occur northeast of the G-node of DONET2 and are spatiotemporally correlated with VLFs. Most of these tremors are at the peak of the subducted seamount along the dip direction; therefore, a spatial relationship between slow earthquakes and a seamount is suggested.

Overall, the dense observation of DAS measurement enabled us to reveal the detailed characteristics of tremor signals. In this observation, the number of events was small and VLFs were not observed in the low frequency band. In future works, DAS measurement with a longer sensing length and lower noise level in the VLFE frequency band is required. As the longer duration of tremor signals in DAS channels may be caused by the sensitivity of the incident angle or lower velocity of *S*-coda phases, the cause of the difference between the waveforms of DAS and seismometers should also be investigated.

Data Availability Statement

The tremor and VLFE lists constructed in this study (Data Set S1–S3), DAS channel position information, and the DAS data of tremors (hdf5 files) are available online (<https://doi.org/10.5281/zenodo.7935235>). We used generic mapping tools (Wessel et al., 2013) and Seismic Analysis Code (Helffrich et al., 2013) to prepare figures and process seismograms, respectively. We used DONET broadband seismograms (<https://hinetwww11.bosai.go.jp/auth/download/cont/?LANG=en>; Registration is required to download).

Acknowledgments

We would like to thank the Editor Daoyuan Sun and two reviewers for valuable comments and suggestions. This research was supported by JSPS KAKENHI Grant-in-Aid for Scientific Research on Transformative Research Areas (A) "Science of Slow-to-Fast earthquakes" (JP21H05204) and Grant-in-Aid for Research Activity Start-up (JP22K20394). We thank Editage (www.editage.com) for English language editing.

References

- Amante, C., & Eakins, B. W. (2009). *ETOPO1 1 Arc-minute global relief model: Procedures, data sources and analysis* (Vol. 24). NOAA Technical Memorandum NESDIS NGDC. <https://doi.org/10.7289/V5C8276M>
- Ando, M. (1975). Source mechanisms and tectonic significance of historical earthquakes along the Nankai trough, Japan. *Tectonophysics*, 27(2), 119–140. [https://doi.org/10.1016/0040-1951\(75\)90102-X](https://doi.org/10.1016/0040-1951(75)90102-X)
- Aoi, S., Asano, Y., Kunugi, T., Kimura, T., Uehira, K., Takahashi, N., et al. (2020). MOWLAS: NIED observation network for earthquake, tsunami and volcano. *Earth Planets and Space*, 72(1), 126. <https://doi.org/10.1186/s40623-020-01250-x>
- Daley, T. M., Miller, D. E., Dodds, K., Cook, P., & Freifeld, B. M. (2016). Field testing of modular borehole monitoring with simultaneous distributed acoustic sensing and geophone vertical seismic profiles at Citronelle, Alabama. *Geophysical Prospecting*, 64(5), 1318–1334. <https://doi.org/10.1111/1365-2478.12324>
- Dragert, H., Wang, K., & James, T. S. (2001). A silent slip event on the deeper Cascadia subduction interface. *Science*, 292(5521), 1525–1528. <https://doi.org/10.1126/science.1060152>
- Earthquake Research Committee. (2001). Long-term evaluation of earthquakes in the Nankai Trough report. (in Japanese).
- Helffrich, G., Wookey, J., & Bastow, I. (2013). *The seismic analysis code*. Cambridge University Press. <https://doi.org/10.1017/CBO9781139547260>
- Hirose, H., Hirahara, K., Kimata, F., Fujii, N., & Miyazaki, S. (1999). A slow thrust slip event following the two 1996 Hyuganada earthquakes beneath the Bungo Channel, southwest Japan. *Geophysical Research Letters*, 26(21), 3237–3240. <https://doi.org/10.1029/1999GL010999>
- Ide, S. (2010). Striations, duration, migration and tidal response in deep tremor. *Nature*, 466(7304), 356–359. <https://doi.org/10.1038/nature09251>
- Ide, S., Araki, E., & Matsumoto, H. (2021). Very broadband strain-rate measurements along a submarine fiber-optic cable off Cape Muroto, Nankai subduction zone, Japan. *Earth Planets and Space*, 73(1), 63. <https://doi.org/10.1186/s40623-021-01385-5>
- Ide, S., Beroza, G. C., Shelly, D. R., & Uchide, T. (2007). A scaling law for slow earthquakes. *Nature*, 447(7140), 76–79. <https://doi.org/10.1038/nature05780>
- Ito, Y., Obara, K., Shiomi, K., Sekine, S., & Hirose, H. (2007). Slow earthquakes coincident with episodic tremors and slow slip events. *Science*, 315(5811), 503–506. <https://doi.org/10.1126/science.1134454>
- Kaneda, Y., Kawaguchi, K., Araki, E., Matsumoto, H., Nakamura, T., Kamiya, S., et al. (2015). Development and application of an advanced ocean floor network system for megathrust earthquakes and tsunamis. In P. Favali, L. Beranzoli, & A. D. Santis (Eds.), *Seafloor observatories* (pp. 643–663). Springer. https://doi.org/10.1007/978-3-642-11374-1_25
- Kaneko, L., Ide, S., & Nakano, M. (2018). Slow earthquakes in the microseism frequency band (0.1–1.0 Hz) off Kii Peninsula, Japan. *Geophysical Research Letters*, 45(6), 2618–2624. <https://doi.org/10.1002/2017GL076773>
- Kato, A., Obara, K., Igarashi, T., Tsuruoka, H., Nakagawa, S., & Hirata, N. (2012). Propagation of Slow slip leading up to the 2011 Mw 9.0 Tohoku-Oki earthquake. *Science*, 335(6069), 705–708. <https://doi.org/10.1126/science.1215141>
- Kodaira, S., Takahashi, N., Nakanishi, A., Miura, S., & Kaneda, Y. (2000). Subducted seamount imaged in the rupture zone of the 1946 Nankaido Earthquake. *Science*, 289(5476), 104–106. <https://doi.org/10.1126/science.289.5476.104>
- Lindsey, N. J., Martin, E. R., Dreger, D. S., Freifeld, B., Cole, S., James, S. R., et al. (2017). Fiber-optic network observations of earthquake wavefields. *Geophysical Research Letters*, 44(23), 11792–11799. <https://doi.org/10.1002/2017GL075722>
- Lior, I., Sladen, A., Rivet, D., Ampuero, J. P., Hello, Y., Becerril, C., et al. (2021). On the detection capabilities of underwater distributed acoustic sensing. *Journal of Geophysical Research: Solid Earth*, 126(3), e2020JB020925. <https://doi.org/10.1029/2020JB020925>
- Masuda, K., Ide, S., Ohta, K., & Matsuzawa, T. (2020). Bridging the gap between low-frequency and very-low-frequency earthquakes. *Earth Planets and Space*, 72(1), 47. <https://doi.org/10.1186/s40623-020-01172-8>
- Matsumoto, H., Araki, E., Kimura, T., Fujie, G., Shiraishi, K., Tonegawa, T., et al. (2021). Detection of hydroacoustic signals on a fiber-optic submarine cable. *Scientific Reports*, 11(1), 2797. <https://doi.org/10.1038/s41598-021-82093-8>
- Nakamura, Y., Shiraishi, K., Fujie, G., Kodaira, S., Kimura, G., Kaiho, Y., et al. (2022). Structural anomaly at the boundary between strong and weak plate coupling in the central-western Nankai trough. *Geophysical Research Letters*, 49(10), e2022GL098180. <https://doi.org/10.1029/2022GL098180>
- Nakanishi, A., Takahashi, N., Yamamoto, Y., Takahashi, T., Ozgur Citak, S., Nakamura, T., et al. (2018). Three-dimensional plate geometry and P-wave velocity models of the subduction zone in SW Japan: Implications for seismogenesis. In T. Byrne, M. B. Underwood III, et al. (Eds.), *Geology and tectonics of subduction zones: A tribute to Gaku Kimura, Special Paper of the Geological Society of America* (Vol. 534). [https://doi.org/10.1130/2018.2534\(04\)](https://doi.org/10.1130/2018.2534(04))
- Nakano, M., Hori, T., Araki, E., Kodaira, S., & Ide, S. (2018). Shallow very-low-frequency earthquakes accompany slow slip events in the Nankai subduction zone /704/2151/210 /704/2151/508 article. *Nature Communications*, 9(1), 984. <https://doi.org/10.1038/s41467-018-03431-5>
- Nakano, M., Nakamura, T., Kamiya, S. N. I., Ohori, M., & Kaneda, Y. (2013). Intensive seismic activity around the Nankai trough revealed by DONET ocean-floor seismic observations. *Earth Planets and Space*, 65(1), 5–15. <https://doi.org/10.5047/eps.2012.05.013>
- National Research Institute for Earth Science and Disaster Resilience. (2019). NIED DONET. <https://doi.org/10.17598/NIED.0008>
- Obara, K. (2002). Nonvolcanic deep tremor associated with subduction in southwest Japan. *Science*, 296(5573), 1679–1681. <https://doi.org/10.1126/science.1070378>
- Obara, K., & Ito, Y. (2005). Very low frequency earthquakes excited by the 2004 off Kii peninsula earthquakes: A dynamic deformation process in the large accretionary prism. *Earth Planets and Space*, 57(4), 321–326. <https://doi.org/10.1186/BF03352570>
- Obara, K., & Kato, A. (2016). Connecting slow earthquakes to huge earthquakes. *Science (New York, N.Y.)*, 353(6296), 253–257. <https://doi.org/10.1126/science.aaf1512>
- Shinohara, M., Yamada, T., Akuhara, T., Mochizuki, K., & Sakai, S. (2022). Performance of seismic observation by distributed acoustic sensing technology using a seafloor cable off Sanriku, Japan. *Frontiers in Marine Science*, 9. <https://doi.org/10.3389/fmars.2022.844506>
- Sun, T., Saffer, D., & Ellis, S. (2020). Mechanical and hydrological effects of seamount subduction on megathrust stress and slip. *Nature Geoscience*, 13(3), 249–255. <https://doi.org/10.1038/s41561-020-0542-0>
- Takemura, S., Matsuzawa, T., Noda, A., Tonegawa, T., Asano, Y., Kimura, T., & Shiomi, K. (2019). Structural characteristics of the Nankai trough shallow plate boundary inferred from shallow very low frequency earthquakes. *Geophysical Research Letters*, 46(8), 4192–4201. <https://doi.org/10.1029/2019GL082448>
- Takemura, S., Obara, K., Shiomi, K., & Baba, S. (2022). Spatiotemporal variations of shallow very low frequency earthquake activity southeast off the Kii Peninsula, along the Nankai trough, Japan. *Journal of Geophysical Research: Solid Earth*, 127(3), e2021JB023073. <https://doi.org/10.1029/2021JB023073>
- Tamaribuchi, K., Ogiso, M., & Noda, A. (2022). Spatiotemporal distribution of shallow tremors along the Nankai trough, Southwest Japan, as determined from waveform amplitudes and cross-correlations. *Journal of Geophysical Research: Solid Earth*, 127(8), e2022JB024403. <https://doi.org/10.1029/2022JB024403>

- Toh, A., Chen, W. J., Takeuchi, N., Dreger, D. S., Chi, W. C., & Ide, S. (2020). Influence of a subducted oceanic ridge on the distribution of shallow VLFs in the Nankai trough as revealed by moment tensor inversion and cluster analysis. *Geophysical Research Letters*, *47*(15), e2020GL087244. <https://doi.org/10.1029/2020GL087244>
- Tonegawa, T., Araki, E., Matsumoto, H., Kimura, T., Obana, K., Fujie, G., et al. (2022). Extraction of P wave from ambient seafloor noise observed by distributed acoustic sensing. *Geophysical Research Letters*, *49*(4), e2022GL098162. <https://doi.org/10.1029/2022GL098162>
- Vaca, S., Vallée, M., Nocquet, J. M., Battaglia, J., & Régnier, M. (2018). Recurrent slow slip events as a barrier to the northward rupture propagation of the 2016 Pedernales earthquake (Central Ecuador). *Tectonophysics*, *724–725*, 80–92. <https://doi.org/10.1016/j.tecto.2017.12.012>
- Wang, H. F., Zeng, X., Miller, D. E., Fratta, D., Feigl, K. L., Thurber, C. H., & Mellors, R. J. (2018). Ground motion response to an ML 4.3 earthquake using co-located distributed acoustic sensing and seismometer arrays. *Geophysical Journal International*, *213*(3), 2020–2036. <https://doi.org/10.1093/GJI/GGY102>
- Wessel, P., Smith, W. H. F., Scharroo, R., Luis, J., & Wobbe, F. (2013). Generic mapping tools: Improved version released. *Eos*, *94*(45), 409–410. <https://doi.org/10.1002/2013EO450001>
- Williams, E. F., Fernández-Ruiz, M. R., Magalhaes, R., Vanthillo, R., Zhan, Z., González-Herráez, M., & Martins, H. F. (2019). Distributed sensing of microseisms and teleseisms with submarine dark fibers. *Nature Communications*, *10*(1), 5778. <https://doi.org/10.1038/s41467-019-13262-7>
- Yamamoto, Y., Ariyoshi, K., Yada, S., Nakano, M., & Hori, T. (2022). Spatio-temporal distribution of shallow very-low-frequency earthquakes between December 2020 and January 2021 in Kumano-nada, Nankai subduction zone, detected by a permanent seafloor seismic network. *Earth Planets and Space*, *74*(1), 14. <https://doi.org/10.1186/s40623-022-01573-x>
- Yamashita, Y., Shinohara, M., & Yamada, T. (2021). Shallow tectonic tremor activities in Hyuga-nada, Nankai subduction zone, based on long-term broadband ocean bottom seismic observations. *Earth Planets and Space*, *73*(1), 196. <https://doi.org/10.1186/s40623-021-01533-x>
- Yokota, Y., & Ishikawa, T. (2020). Shallow slow slip events along the Nankai Trough detected by GNSS-A. *Science Advances*, *6*(3), 1–12. <https://doi.org/10.1126/sciadv.aay5786>
- Zhan, Z. (2019). Distributed acoustic sensing turns fiber-optic cables into sensitive seismic antennas. *Seismological Research Letters*, *91*(1), 1–15. <https://doi.org/10.1785/0220190112>